

Guiding light at the nanoscale: numerical optimization of ultrasubwavelength metallic wire plasmonic waveguides

Alexey V. Krasavin* and Anatoly V. Zayats

Department of Physics, King's College London, Strand, London WC2R 2LS, UK

*Corresponding author: alexey.krasavin@kcl.ac.uk

Received May 4, 2011; revised June 28, 2011; accepted July 6, 2011;
posted July 8, 2011 (Doc. ID 147080); published August 10, 2011

We present a comprehensive numerical analysis of the guiding of a photonic signal in the form of a strongly confined asymmetric surface plasmon polariton (SPP) mode along metallic nanowire waveguides. The proposed approach provides extremely high localization of the SPP mode, nanoscale integration density, and a feasible technological platform. The waveguide performance was studied over a broad range of subwavelength cross sections at a telecommunication wavelength. It was optimized using a conventional figure of merit for data transfer along a straight waveguide and an all-inclusive figure of merit has been introduced. © 2011 Optical Society of America
OCIS codes: 130.0130, 250.5403.

Surface plasmon polaritons (SPPs) offer a unique opportunity to localize and guide photonic signals on the nanoscale. Recently, truly nanoscale guiding along the gap, nanoparticle chain, dielectric-loaded, or circular nanowire plasmonic waveguides have been demonstrated [1–3]. In this Letter, we investigate guiding a photonic signal in the form of an asymmetric SPP mode along a nanoscale metallic wire waveguides with multifarious rectangular cross sections. This approach can provide extremely high field localization and nanoscale integration density along with a feasible technological platform which allows the incorporation of signal amplification. These are key advantages in comparison with the other types of SPP waveguides. The incorporation of such broadband photonic waveguides into electronic circuits opens a prospective solution to the problem of electronic interconnect bottleneck, leading to the realization of hybrid electronic/photonic circuits.

The asymmetric plasmonic mode in a metallic wire waveguide (Fig. 1) [3,4], in contrast its symmetric long-range large-size counterpart [5], has not been intensively studied until very recently, when an approach for its efficient excitation was found [6]. This mode is extremely promising in terms of achieving strong field localization and high-density photonic integration. Furthermore, it does not have a cutoff in terms of the waveguide cross section and the smaller the waveguide size, the higher the localization of the mode—exactly what is needed to achieve nanoscale integration density. However, as usual for SPP modes, there is a trade-off between localization and propagation characteristics, depending in this case on the waveguide geometrical parameters. This leads to the question of what is the best waveguide cross section for specific nanophotonic applications. In this Letter, the guiding properties of such waveguides have been investigated over a wide range of subwavelength cross sections to determine both the optimal parameters for data transfer through a straight waveguide and separately, for multibranch SPP circuits.

We have studied nanowire waveguides having a rectangular cross section embedded in an InGaAsP-based

medium [Fig. 1(a)]. The wavelength was chosen as $\lambda = 1550$ nm to target the possible application of the waveguides in telecommunications. The choice of noble metal insures longer propagation distance, while an appropriate choice of dielectric enables the introduction of gain, compensating the losses in metal and increasing the SPP signal propagation length [7]. The refractive indices for gold ($n_1 = 0.55 - 11.5i$) and InGaAsP ($n_2 = 3.37$) were taken from [8] and [9], respectively. We performed two-dimensional eigenmode numerical simulations of the system using COMSOL Multiphysics software. Special care was made for proper meshing (2.5 nm mesh in the waveguide core area, 37.5 nm in the coating), sufficient distance to the outer domain boundaries (5 μ m), and dense enough mode mapping to ensure correct simulation of the mode and correct calculation of its parameters. Numerical simulations reveal that for the dimensions of interest in this work, the waveguide is a single mode for modes with an asymmetric field distribution. The supported asymmetric mode is localized in a region of a few tens of nanometers next to the waveguide surface [Fig. 1(a)]. Its electric field is directed radially from (or to, half an optical cycle later) the center of the waveguide.

The mode behavior has been investigated for a wide range of waveguide cross sections, with particular emphasis on ultrasubwavelength dimensions, down to a 25 nm \times 25 nm size. The width of the waveguide, w , and height, h , were continually varied, while the main mode characteristics: effective refractive index n_{eff} , effective mode area S_{eff} , and propagation length L_{prop} were monitored. The mode effective refractive index was defined as $n_{\text{eff}} = k_{\text{SPP}}^{\text{mode}}/k$, where $k = 2\pi/\lambda$ is the free space wave vector. The effective area was defined as an area inside the constant magnitude contour, encircling $(1 - 3e^{-2})$ part (around 60%) of the total intensity integral in the dielectric, plus the area of the metal section supporting it (see the inset to [Fig. 1(b)]) [9]. This part of the energy is encircled by the $1/e$ field decay contour in the case of the Gaussian mode distribution. Here we used an integral (in contrast to a magnitude as in [10]) condition for the level defining the contour, because with various

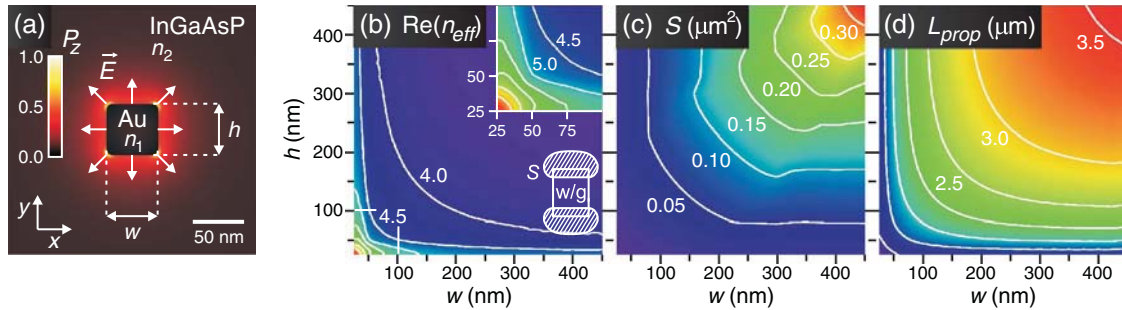


Fig. 1. (Color online) (a) Field map of power flow P_z of the asymmetric SPP mode at $\lambda = 1550$ nm, supported by a 50 nm \times 50 nm Au waveguide embedded in InGaAsP. The dependences of the (b) real part of the mode effective refractive index, (c) effective mode area, and (d) propagation length of the mode on waveguide geometrical parameters.

waveguide cross sections, various mode profiles should be expected. According to the investigation specifically devoted to various methods of estimating the effective area of the plasmonic modes [11], this approach is the most reliable for application to different plasmonic waveguides. The propagation length $L_{\text{prop}} = \lambda / (4\pi \text{Im}(n_{\text{eff}}))$ was defined as the distance at which the energy of the mode decreases by a factor of e . The corners of the waveguide were rounded with a radius of $r = 5$ nm to avoid field singularities and also due to the fact that this is usually the case in practice.

The behavior of the asymmetric mode is totally opposite to that of the symmetric one described in [9]. The smaller waveguide size corresponds to the higher effective refractive index [Fig. 1(b)] and the greater mode localization [Fig. 1(c)]. For waveguides with lateral dimensions around 25 nm, the real part of the effective refractive index reaches values higher than 7.5 , which makes these waveguides very promising in terms of photonic circuit integration. Such a large effective index lowers the minimum bending radius achievable before the mode couples to photons at the outer edge of the bend. Furthermore, power flow is localized just 15 nm from the waveguide surface (corresponding to the mode size of 50 nm). The typical power flow map for the case of a 50 nm \times 50 nm waveguide is presented in Fig. 1(a). As usual, there is a trade-off between its localization and propagation characteristics. In modes of a smaller size, the electromagnetic fields are pushed into the metal, which increases the ohmic losses and decreases the propagation length below 1 μm . The same highly localized behavior is observed when either side of the waveguide is in the region of 25 – 50 nm, although the two regions of mode localization are then well separated [Fig. 2(a)]. At the other side of the waveguide sizes $w \sim h \sim 450$ nm, the mode becomes decomposed into a set of practically isolated wedge SPP modes with $L_{\text{prop}} = 3.6$ μm . As expected from the mode symmetry, all of the graphs are symmetric with respect to the diagonal $w = h$ axis. Finally, it was found that the group velocity dispersion (GVD) for the smallest waveguide (25 nm \times 25 nm) is ~ 0.1 ps²/mm, making the waveguides practically nondispersive at the operation length scale.

To find an optimal waveguide cross section in terms of mode localization/propagation trade-off in the case of guiding along a straight waveguide, a figure of merit $M_1 = 2\sqrt{\pi}L_{\text{prop}}/\sqrt{S}$ [10] has been implemented. M_1 is a straightforward ratio between the propagation length

L_{prop} , reflecting the propagation characteristic of the mode and the size of the mode \sqrt{S} , reflecting its localization. The parametric plot of the figure of merit reveals that there is a clear optimum of the waveguide performance at a size of 125 nm \times 125 nm [Fig. 2(b)]. The two maximum regions at higher values of width or height are less interesting, since having the same value of M_1 , they correspond to weaker localization, the key advantage of this SPP mode. If active functionalities based on the coating medium are not needed, then low refractive index coating (e.g., silica or polymer) is advantageous. For example, a 68 nm \times 68 nm silica-coated waveguide with the same mode area (0.026 μm^2) as a 125 nm \times 125 nm InGaAsP-coated waveguide has a 2.5 times larger propagation length. The M_1 in this case represents a plateau at the level of 130 at $w, h > 100$ nm, decreasing with a sharp gradient towards 90 at the axis $w = 25$ nm and $h = 25$ nm. Careful comparison of the modes will be reported elsewhere.

The effective mode size included in M_1 gives valid estimation about the possible integration density. At the same time, the exact answer will only be given by a direct evaluation of the cross talk between the waveguides. Following [2], the figure of merit was modified such that $M_1^* = L_{\text{prop}}/d$, where d is the waveguide center-to-center separation required for a certain coupling length L_{coupl} , corresponding to the distance at which the mode initially launched in one waveguide is fully transferred to another one, and placed parallel to it (25% of the mode energy is transferred after $L_{\text{coupl}}/3$). It was calculated from the

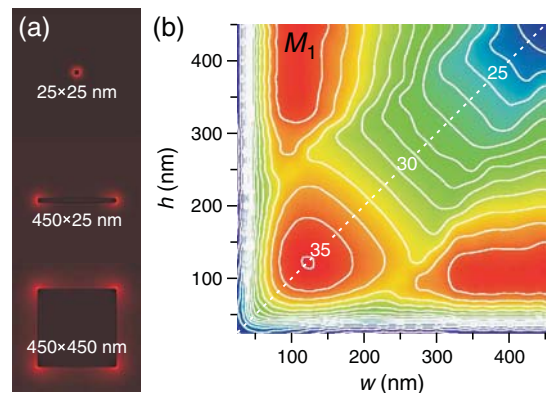


Fig. 2. (Color online) (a) Maps of power flow along the waveguide for 25 nm \times 25 nm, 450 nm \times 25 nm, and 450 nm \times 450 nm waveguides. (b) Figure of merit M_1 as a function of waveguide geometrical parameters.

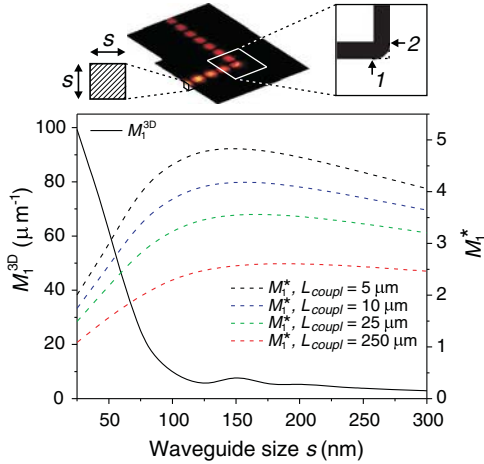


Fig. 3. (Color online) Modified figures of merit M_1^{3D} (solid black curve) and M_1^* (defined for $L_{\text{coupl}} = 5 \mu\text{m}$ dashed black curve, $L_{\text{coupl}} = 10 \mu\text{m}$ dashed blue curve, $L_{\text{coupl}} = 25 \mu\text{m}$ dashed green curve, $L_{\text{coupl}} = 250 \mu\text{m}$ dashed red curve) as functions of waveguide size s for waveguides of a square cross section. The top insets show the $|\text{Re}(E_y)|$ map of the mode transmission through a bend along with the vertical cross section of a waveguide and a horizontal cross section of the bend.

difference between the effective refractive indexes of the symmetric and asymmetric modes found in two-dimensional eigenmode simulations of the coupled double-waveguide system. The dependence of M_1^* on the waveguide size for the waveguides of a square cross section is presented in Fig. 3 for various values of L_{coupl} . Initially, the modified figures of merit increase with waveguide size, but then at $s \sim 125$ nm they reach their maximal values. Notably, for square waveguides the qualitative behavior of M_1^* is rather independent of the particular choice of L_{coupl} .

The performance of the waveguide was further investigated in terms of its implementation in multibranch plasmonic circuits. The efficiency of the waveguide bend is important in this case, since this ultimately defines the size of all circuit elements and therefore the possible photonic integration density. To estimate this, sets of full-vectorial three-dimensional (3D) numerical simulations were performed for the waveguides with square cross sections [indicated by a dashed line in Fig. 2(b)]. For each cross section, a 90° waveguide bend was simulated, continually varying the bending radius (the radius of the waveguide central axis) and monitoring the SPP transmission. Plotted in Fig. 3 is a modified figure of merit $M_1^{3D} = L_{\text{prop}}/d \cdot (T/r)_{\text{max}}$ adapted from [2], where $(T/r)_{\text{max}}$ is the maximum value of transmission-to-radius ratio found in 3D simulations and d is the separation corresponding to $L_{\text{coupl}} = 25 \mu\text{m}$ calculated before.

Transmission T was calculated as a ratio of mode energies just before and just after the bend (positions 1 and 2 in Fig. 3, inset). The maximum in the total efficiency is observed at smaller cross sections $s < 50$ nm, having higher mode effective refractive indices; this follows as expected from our previous discussion. Moreover, for them the highest transmission (reaching $T = 0.8$ – 0.9 for $s = 25$ – 40 nm) occurs when the bending radius is equal to half of the waveguide width, corresponding to the case of a zero radius inner edge (see inset to Fig. 3, solid black shape). This behavior of the figure of merit is essentially important, since in many cases smaller waveguide cross sections correspond to the lower integration characteristics due to the increased mode area. Finally, we note that it is even possible to bend a waveguide with a sharp-corner bend (see inset, dashed line), for a $25 \text{ nm} \times 25 \text{ nm}$ waveguide the transmission is $T = 0.74$.

In conclusion, we have performed a comprehensive numerical analysis of the guiding of a photonic signal in the form of an asymmetric SPP mode along metallic nanowire waveguides. The performance of the waveguide was investigated for a whole range of ultrashort-wavelength waveguide cross sections, monitoring all the mode guiding characteristics. The best waveguide cross section in terms of the mode localization/propagation trade-off was found to be $125 \text{ nm} \times 125 \text{ nm}$. Furthermore, introducing an all-inclusive figure of merit, the high potential of these low GVD waveguides for implementation in highly integrated photonic circuits has been revealed.

This work was supported by the UK Engineering and Physical Sciences Research Council (EPSRC).

References

1. S. I. Bozhevolnyi, ed., *Plasmonic Nanoguides and Circuits* (Pan Stanford, 2008).
2. A. V. Krasavin and A. V. Zayats, *Opt. Express* **18**, 11791 (2010).
3. J. Takahara, S. Yamagishi, H. Taki, A. Morimoto, and T. Kobayashi, *Opt. Lett.* **22**, 475 (1997).
4. J. Jung, T. Sondergaard, and S. I. Bozhevolnyi, *Phys. Rev. B* **76**, 035434 (2007).
5. P. Berini, *Phys. Rev. B* **61**, 10484 (2000).
6. E. Verhagen, M. Spasenovic, A. Polman, and L. (Kobus) Kuipers, *Phys. Rev. Lett.* **102**, 203904 (2009).
7. M. Nezhad, K. Tetz, and Y. Feinman, *Opt. Express* **12**, 4072 (2004).
8. E. D. Palik, ed., *Handbook of Optical Constants of Solids* (Academic, 2010).
9. A. V. Krasavin and A. V. Zayats, *Opt. Lett.* **35**, 2118 (2010).
10. R. Buckley and P. Berini, *Opt. Express* **15**, 12174 (2007).
11. R. F. Oulton, G. Bartal, D. F. P. Pile, and X. Zhang, *New. J. Phys.* **10**, 105018 (2008).